

# AUTOMOTIVE RADAR INTERFERENCE MITIGATION VIA SINR MAXIMIZATION

Shuai Yang, \*Dongheng Zhang, Jinbo Chen, Fang Zhou, Guanzhong Wang, Qibin Sun and Yan Chen

School of Cyber Science and Technology, University of Science and Technology of China, Hefei, China

## ABSTRACT

The mutual interference mitigation between identical or similar radar systems in autonomous driving has gained wide spread attention from both academia and industry. The resulted ghost target interference will reduce the sensitivity of the radar sensor and increase the false alarm rate. To tackle this problem, in this paper, we make full use of two characteristics of interference to achieve ghost target interference mitigation in the Doppler domain. The key insight lies in the fact that the interference is one-way propagation, and thus the resulted ghost target can be converted to the noise floor in the Doppler domain through random slow-time coding. Moreover, the high power characteristic of interference allows us to further enhance the interference mitigation performance by adopting a signal-to-interference-plus-noise ratio (SINR) maximization principle. Numerical examples are provided to demonstrate the effectiveness of the proposed interference mitigation approach.

**Index Terms**— Automotive radar, interference mitigation, SINR maximization, slow-time coding

## 1. INTRODUCTION

Millimeter-wave radar has been widely used in autonomous driving, due to its characteristics of low price and immunity to adverse weather conditions [1, 2, 3, 4, 5, 6, 7, 8]. Given the tendency to mass-produce radars for automobile applications, such systems tend to be quite similar, or even almost identical. The increasing number of similar or identical radar systems increases the probability of mutual interference (referred to as ghost target) and severely reduce the sensitivity of the radar sensor [9, 10, 11, 12]. Although ghost targets are rare, they concern automotive manufacturers, since they are hard to be distinguished from real targets and may trigger unwanted reactions in autonomous driving such as emergency breaks and automatic steering [13, 14, 15]. Thus, it is of great importance to tackle this problem.

The mutual interference mitigation has been widely discussed in the existing literature. In [16], an adaptive noise

canceller is proposed for mutual interference suppression by exploiting the different distributions of frequency spectra of target echoes and interference. The Burg's method [17] can be used to extrapolate the disturbed samples. By exploiting the differences between the target echo signals and the interference, the interference mitigation problem can be reformulated as a signal separation problem [18]. A wavelet denoising based algorithm is proposed in [19]. However, aforementioned methods mainly focus on common chirp-like interference, and fail to effectively mitigate the ghost target interference between identical radar systems.

Recently, the authors in [20, 21] focus on the mutual interference between identical radar systems and propose to solve this problem through precise waveform design. However, waveform design usually requires high computational complexity, especially for long code sequence. Besides, given the length of the code sequence, the number of codes with good auto-correlation characteristics is determined, which limits their large-scale use. Moreover, the code sequence used in different radars need to be arranged in advance, which is also not practical in current road scenarios. These limitations remind us to use random code sequences to achieve ghost target interference mitigation.

In this paper, we address the mutual interference mitigation between similar or identical radar systems by making full use of two important characteristics of interference. The key insight lies in the fact that the interference is one-way propagation, and thus the resulted ghost target interference can be converted to the noise floor in the Doppler domain through random slow-time coding. Moreover, the high power characteristic of interference allows us to further enhance the interference mitigation performance by adopting a signal-to-interference-plus-noise ratio (SINR) maximization principle. Compared with existing coding-based methods, our method does not require precise waveform design or collaboration between radar systems, which can be directly used in practice. Numerical examples are provided to demonstrate the effectiveness of the proposed interference mitigation approach.

## 2. PROBLEM FORMULATION

Consider there are two identical radar systems working in the same frequency band, and use frequency modulated continuous wave (FMCW) for their transmission, as shown in Fig. 1.

\*Dongheng Zhang is the corresponding author. This work was supported by National Natural Science Foundation of China under Grant 62201542, National Key R&D Programmes under Grant 2022YFC2503405 and 2022YFC0869800.

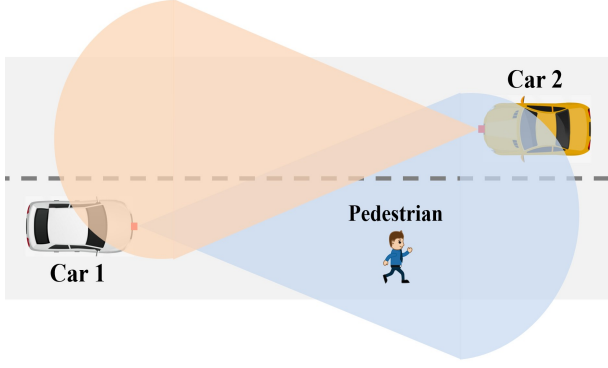


**Fig. 1.** An illustration of mutual interference between automotive radar systems in a road scenario.

In each radar coherent processing interval (CPI),  $N$  chirps are periodically transmitted with a pulse repetition interval (PRI) denoted by  $T$ . Then, the periodic transmitted signal in a CPI can be formulated as:

$$x(t) = \sum_{n=0}^{N-1} u(t - nT) \quad (1)$$

where  $u(t) = \alpha_t e^{j2\pi(f_0 t + \frac{1}{2}\mu t^2)}$ ;  $\alpha_t$  is the amplitude of the transmitted signal;  $\mu = B/T$  is the slope defined by the ratio of bandwidth  $B$  and chirp duration  $T$ . Here, the sweep bandwidth  $B$  and the chirp duration  $T$  of the two identical radars are the same.

Assuming that there are  $K$  targets in the filed of interest, and the round trip time delay corresponding to the  $k^{\text{th}}$  target is:

$$\tau_k = \frac{2(r_k + v_k t)}{c} \quad (2)$$

where  $r_k, v_k$  denote the distance and radial velocity of the  $k^{\text{th}}$  target. The received signal  $s(t)$  is a time-delay version of the transmitted signal  $x(t)$ , and can be written as:

$$s(t) = \sum_{k=1}^K \alpha_k x(t - \tau_k) \quad (3)$$

where  $\alpha_k$  is the amplitude corresponding to the  $k^{\text{th}}$  target, which is proportional to the radar cross section (RCS).

In addition to target echo, there also exists the interference signal coming from the aggressor radar. Similar to (1), the aggressor radars also transmit periodic chirps, and after one-way propagation, the interference signal arriving at the receiver of the victim radar can be expressed as:

$$i(t) = \alpha_I x(t - \tau_I) \quad (4)$$

where

$$\tau_I = \frac{r_I + v_I t}{c} \quad (5)$$

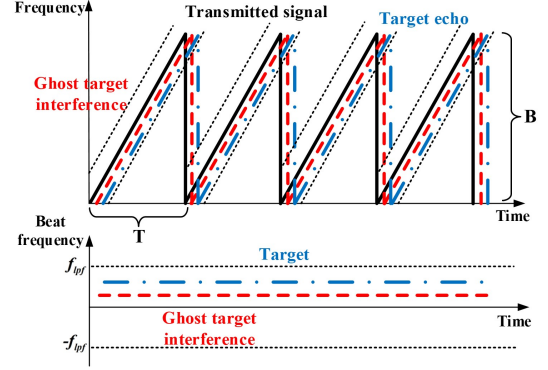


**Fig. 2.** The time-frequency diagram of the FMCW radar affected by an identical radar system.

is the time delay between the aggressor radar and the victim radar;  $\alpha_I$  denotes the amplitude of the interference signal;  $r_I$  and  $v_I$  represent the distance and the radial velocity between the aggressor and victim radar, respectively.

At the receiver of the victim radar, the received signal  $y(t)$  is the sum of the target echo  $s(t)$  and the interference signal  $i(t)$ :

$$r(t) = s(t) + i(t) + e(t) \quad (6)$$

where  $e(t)$  denotes the zero-mean circularly symmetric complex-valued Gaussian white noise with variance  $\delta^2$ . Then, the received signal  $r(t)$  is mixed with the complex conjugate of the transmitted signal  $u(t)$ . This procedure, referred to as dechirping, yields a demodulated signal (beat signal) given by  $y(t) = r(t) \cdot u^*(t)$ . The beat signal after low-pass filtering can be approximately written as:

$$y(t) = \sum_{k=1}^K \tilde{\alpha}_k e^{-j2\pi \left[ \left( \frac{2Br_k}{Tc} + \frac{2f_0 v_k}{c} \right) t + \frac{2f_0 v_k T}{c} q \right]} + \tilde{\alpha}_I e^{-j2\pi \left[ \left( \frac{Br_I}{Tc} + \frac{f_0 v_I}{c} \right) t + \frac{2f_0 v_I T}{c} q \right]} + \tilde{e}(t), \quad (7)$$

where  $\tilde{\alpha}_k = \alpha_k \alpha_t e^{-j2\pi f_0 \frac{2r_k}{c}}$ ,  $\tilde{\alpha}_I = \alpha_I \alpha_t e^{-j2\pi f_0 \frac{r_I}{c}}$  and  $\tilde{e}(t) = e(t) \cdot u^*(t)$ .

Let  $f_s$  denote the sampling frequency to sample the received signal, then the signal model in Eq. (7) becomes:

$$y(n, m) = \sum_{k=1}^K \tilde{\alpha}_k e^{-j2\pi (f_{r,k} m + f_{d,k} n)} + \tilde{\alpha}_I e^{-j2\pi (f_{r,I} m + f_{d,I} n)} + \tilde{e}(n, m) \quad (8)$$

where  $n = 1, \dots, N$  and  $m = 1, \dots, M$  represent the slow-time and fast-time index, respectively.

### 3. METHODS

In this section, we make full use of two important characteristics of interference, one-way propagation and high power, to achieve ghost target interference mitigation.

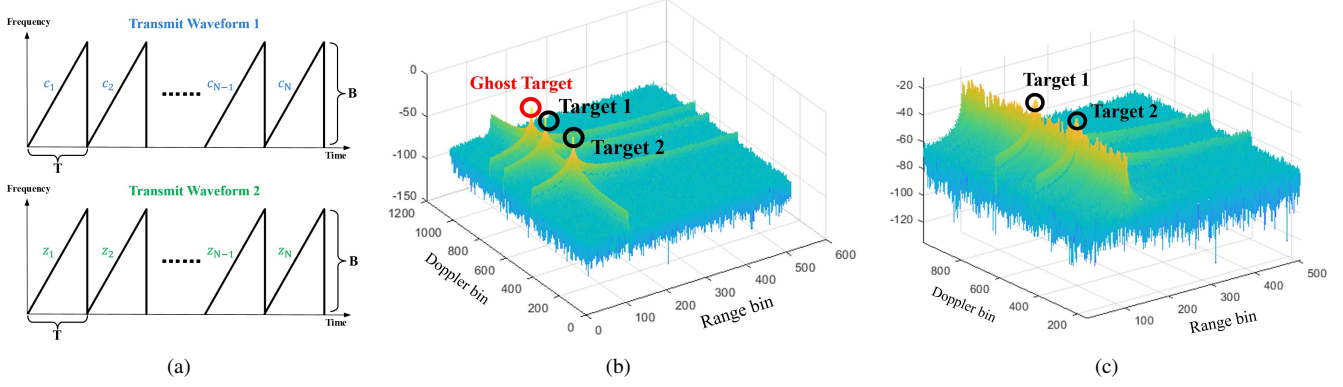


**Fig. 3.** (a). An illustration of slow-time coding. (b). The ghost target interference in the range-Doppler domain without slow-time coding. (c). After slow-time coding, the ghost target becomes the noise floor in the Doppler domain. Here, the target echo of interest and the ghost target is marked with black and red circle, respectively.

Since the interference is one-way propagation, while the target echo experiences two-way round trips, it is natural to use coding-based methods to separate interference from the target echo. However, existing coding-based methods not only have high computational complexity, but also require collaboration between different radars, and cannot be directly used in modern road scenarios. These limitations remind us to use random code sequences to achieve ghost target interference mitigation.

The random slow-time coding sequence used in a single CPI is illustrated in Fig. 3(a). The coding sequences of the two identical radar systems are denoted as  $\mathbf{c} = [c_1, c_2, \dots, c_N]^T$  and  $\mathbf{z} = [z_1, z_2, \dots, z_N]^T$ . Then, at the transmitter of the victim radar, the transmit signal becomes  $c(n)u(t)$ , and the transmit signal of the aggressor radar is  $z(n)u(t)$ , respectively. To keep constant transmit power over the  $N$  chirps, we constrain the code sequences to be unimodular, i.e.,  $|c_n| = |z_n| = 1, n = 1, 2, \dots, N$ .

At the receiver of the victim radar, after dechirping, the digital data samples in Eq. (8) becomes:

$$y(n, m) = \sum_{k=1}^K \tilde{\alpha}_k e^{-j2\pi(f_{r,k}m + f_{d,k}n)} + \tilde{\alpha}_I c^*(n) z(n) e^{-j2\pi(f_{r,I}m + f_{d,I}n)} + \tilde{e}(n, m). \quad (9)$$

By performing 2-D Fast Fourier Transform (FFT) operation on Eq. (9), we can obtain the corresponding range-Doppler spectrum.

The effect of ghost target interference in the range-Doppler domain with and without slow-time coding is illustrated in Fig. 3(b) and Fig. 3(c). As we can see in Fig. 3(b), without slow-time coding, the interference signal appears as a ghost target in the range-Doppler domain. After slow-time coding, due to the different code sequences used in different radars, the ghost target interference is converted to the noise floor in the Doppler domain, as shown in Fig. 3(c).

Although the ghost target interference disappears, the increased noise floor still reduces the sensitivity of the radar sensor and masks the weak target, and thus needs to be further addressed. We notice that the power of the interference is usually high due to its one-way propagation characteristic. Based on this observation, an efficient SINR maximization principle can be adopted to further eliminate the influence of ghost target interference.

The optimization goal is to find an optimal weight vector  $\mathbf{v} \in \mathbb{C}^{N \times 1}$  to maximize the output SINR in the Doppler domain, as follows:

$$\max_{\mathbf{v}} \frac{P_s}{P_i + P_e} \quad (10)$$

where  $P_s$ ,  $P_i$  and  $P_e$  represent the power of the target echo, interference, and noise;  $P_{i+e} = P_i + P_e = \mathbf{v}^H (\mathbf{R}_i + \mathbf{R}_e) \mathbf{v} = \mathbf{v}^H \mathbf{R}_{i+e} \mathbf{v}$ ;  $\mathbf{R}_i$  and  $\mathbf{R}_e$  denote the covariance matrix of the interference and noise;  $P_s = \alpha_s^2 \mathbf{v}^H \mathbf{a}(f_d) \mathbf{a}^H(f_d) \mathbf{v}$ ;  $\alpha_s^2$  represent the power of input signal;  $\mathbf{a}(f_d) = [1, \dots, e^{-j2\pi f_d(N-1)}]$  is the steering vector in the Doppler domain.

Then, Eq. (10) can be rewritten as:

$$\max_{\mathbf{v}} \frac{\alpha_s^2 \mathbf{v}^H \mathbf{a}(f_d) \mathbf{a}^H(f_d) \mathbf{v}}{\mathbf{v}^H \mathbf{R}_{i+e} \mathbf{v}}. \quad (11)$$

Since matrix  $\mathbf{R}_{i+e}$  is a semi-positive Hermitian matrix, it can be decomposed as:  $\mathbf{R}_{i+e} = \mathbf{L}\mathbf{L}^H$ . Define  $\tilde{\mathbf{v}} = \mathbf{L}\mathbf{v}$  and  $\tilde{\mathbf{a}}(f_d) = \mathbf{L}^{-1} \mathbf{a}(f_d)$ , then Eq. (11) is equivalent to:

$$\max_{\tilde{\mathbf{v}}} \frac{\alpha_s^2 |\tilde{\mathbf{v}} \tilde{\mathbf{a}}(f_d)|^2}{|\tilde{\mathbf{v}}|^2}. \quad (12)$$

According to Rayleigh inequality [22], Eq. (12) obtain the maximum value when:

$$\begin{aligned} \tilde{\mathbf{v}}_{\text{opt}} &= \beta \tilde{\mathbf{a}}(f_d) \\ &= \beta \mathbf{L}^{-1} \mathbf{a}(f_d) \end{aligned} \quad (13)$$

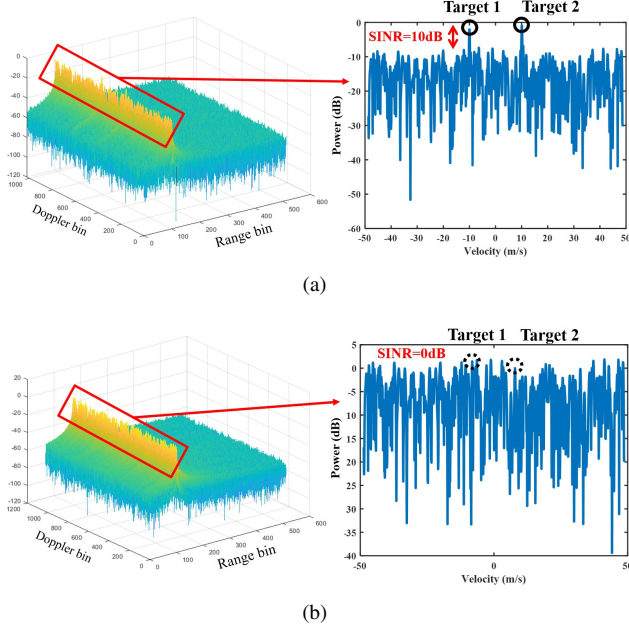


**Fig. 4.** (a). The left picture is the range-Doppler image after slow-time coding when the interference power is 10 dB, and the right picture is the corresponding Doppler spectrum. (b). The interference power is 20 dB, and the target is marked with black dotted circle.

where  $\beta$  is a constant value. Then the optimal weight vector  $\mathbf{v}_{\text{opt}}$  is:

$$\begin{aligned} \mathbf{v}_{\text{opt}} &= \beta(\mathbf{L}^H)^{-1}\mathbf{L}^{-1}\mathbf{a}(f_d) \\ &= \beta\mathbf{R}_{i+e}^{-1}\mathbf{a}(f_d). \end{aligned} \quad (14)$$

Using matrix inverse lemma, Eq. (14) becomes:

$$\begin{aligned} \mathbf{v}_{\text{opt}} &= \beta\mathbf{R}_{i+e}^{-1}\mathbf{a}(f_d) \\ &= \beta \left[ \mathbf{R}_y^{-1} + \frac{\alpha_s^2 \mathbf{R}_y^{-1} \mathbf{a}(f_d) \mathbf{a}^H(f_d) \mathbf{R}_y^{-1}}{1 - \alpha_s^2 \mathbf{a}^H(f_d) \mathbf{R}_y^{-1} \mathbf{a}(f_d)} \right] \mathbf{a}(f_d) \quad (15) \\ &= \beta\mathbf{R}_y^{-1}\mathbf{a}(f_d). \end{aligned}$$

In practice, the true value of the signal covariance matrix  $\mathbf{R}_y$  is hard to obtain, and we usually use the received signal  $\mathbf{y}$  to fit it, e.g.,  $\mathbf{R}_y = \mathbf{y}\mathbf{y}^H$ . Finally, by using the optimal weight vector  $\mathbf{v}_{\text{opt}}$ , we can largely mitigate the influence of the ghost target interference.

#### 4. NUMERICAL EXAMPLES

Consider two identical radars working in the scenario, one as victim radar and the other as aggressor radar. The carrier frequency, chirp bandwidth and chirp duration of the two radars are set to:  $f_c = 77\text{GHz}$ ,  $B = 500\text{MHz}$ ,  $T = 50\mu\text{s}$ , respectively. The chirp number within a single CPI is 256. The sampling frequency is set to  $25\text{MHz}$ , and 512 data samples are collected in a chirp. Then, the size of the received

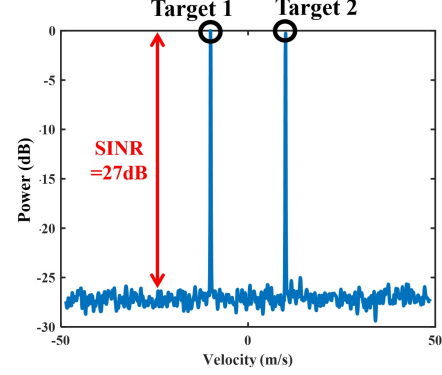


**Fig. 5.** The interference mitigation performance in the Doppler domain after using the proposed method.

signal in a single CPI is  $256 \times 512$ . Assume that there are two targets in the environment, and their range, radial velocity and the corresponding parameters of the aggressor radar are  $\{30\text{m}, 30\text{m}, 30\text{m}\}$ ,  $\{-10\text{m/s}, 10\text{m/s}, 20\text{m/s}\}$ , respectively. The power of both targets is set to  $0\text{dB}$ . Note that the code sequences used in our simulation are all random binary sequences with a modulus of 1. The signal-to-noise ratio (SNR), defined as  $20 \log_{10}\{\alpha_1/\delta\}$ , is set at 10 dB.

After random slow-time coding, the range-Doppler image obtained by 2-D FFT is presented in the left part of Fig. 4(a) and Fig. 4(b). The interference power is  $10\text{dB}$  and  $20\text{dB}$ , respectively. In order to better present the impact of interference in the Doppler domain, we take the Doppler spectrum corresponding to the specific range bin on the right part. Compared with Fig. 3(b), after random slow-time coding, the ghost target is converted to the noise floor in the Doppler domain. The higher the interference power, the higher the increased noise floor, as shown in Fig. 4. Even worse, the increased noise floor caused by interference completely masks the targets in the right part of Fig. 4(b). Then, we deploy the proposed SINR maximization algorithm to tackle this problem, and the obtained Doppler spectrum is presented in Fig. 5. As we can see, the SINR in the Doppler domain is improved to  $27\text{dB}$ , and two masked targets can be reliably detected now.

#### 5. CONCLUSIONS

In this paper, we studied the mutual interference between identical or similar automotive radar systems. By exploiting the one-way propagation and high power characteristics of interference, the ghost target can be efficiently suppressed in the Doppler domain through an SINR maximization principle. Different from existing coding-based methods, our method can work with any random code sequences, which is very suitable for large-scale use. Numerical examples are provided to demonstrate the effectiveness of the proposed interference mitigation algorithm.

## 6. REFERENCES

- [1] Dan Oprisan and Hermann Rohling, "Analysis of mutual interference between automotive radar systems," in *Proc. IEEE Int. Radar Symp.*, 2005.
- [2] Graham M. Brooker, "Mutual interference of millimeter-wave radar systems," *IEEE Trans. Electromagn. Compat.*, vol. 49, no. 1, pp. 170–181, 2007.
- [3] Martin Kunert, "The EU project MOSARIM: A general overview of project objectives and conducted work," in *Proc. Eur. Radar Conf.*, 2012.
- [4] Ruiyuan Song, Dongheng Zhang, Zhi Wu, Cong Yu, Chunyang Xie, Shuai Yang, Yang Hu, and Yan Chen, "RF-URL: unsupervised representation learning for RF sensing," in *Proc. 28th Annu. Int. Conf. Mobile Comput. Netw.*, 2022, pp. 282–295.
- [5] Jinbo Chen, Dongheng Zhang, Zhi Wu, Fang Zhou, Qibin Sun, and Yan Chen, "Contactless electrocardiogram monitoring with millimeter wave radar," *IEEE Trans. Mobile Comput.*, 2022.
- [6] Shuai Yang, Dongheng Zhang, Ruiyuan Song, Pengfei Yin, and Yan Chen, "Multiple WiFi access points colocalization through joint aoa estimation," *IEEE Trans. Mobile Comput.*, 2023.
- [7] Shuai Yang, Xiaolei Shang, Dongheng Zhang, Qibin Sun, and Yan Chen, "IMIA: Interference mitigation via iterative approaches for automotive radar," *IEEE Trans. Radar Systems*, vol. 1, pp. 753–766, 2023.
- [8] Tianyu Zhang, Dongheng Zhang, Shuai Yang, Qibin Sun, and Yan Chen, "WiCo: Robust indoor localization via spectrum confidence estimation," in *IEEE Wireless Commun. Netw. Conf.* IEEE, 2023, pp. 1–6.
- [9] Shuai Yang and Xiaolei Shang, "Iterative approaches to interference mitigation for automotive radar," in *2022 IEEE Radar Conf. (RadarConf22)*. IEEE, 2022, pp. 1–5.
- [10] Shunqiao Sun, Athina P Petropulu, and H Vincent Poor, "MIMO radar for advanced driver-assistance systems and autonomous driving: Advantages and challenges," *IEEE Signal Process. Mag.*, vol. 37, no. 4, pp. 98–117, 2020.
- [11] Stephen Alland, Wayne Stark, Murtaza Ali, and Manju Hegde, "Interference in automotive radar systems: Characteristics, mitigation techniques, and current and future research," *IEEE Signal Process. Mag.*, vol. 36, no. 5, pp. 45–59, 2019.
- [12] Canan Aydogdu, Musa Furkan Keskin, Gisela K Carvajal, Olof Eriksson, Hans Hellsten, Hans Herbertsson, Emil Nilsson, Mats Rydstrom, Karl Vanas, and Henk Wymeersch, "Radar interference mitigation for automated driving: Exploring proactive strategies," *IEEE Signal Process. Mag.*, vol. 37, no. 4, pp. 72–84, 2020.
- [13] Konstantin Hahmann, Stefan Schneider, and Thomas Zwick, "Evaluation of probability of interference-related ghost targets in automotive radars," in *Proc. IEEE MTT-S Int. Conf. Microw. Intell. Mobility (ICMIM)*. IEEE, 2018, pp. 1–4.
- [14] A Bourdoux, K Parashar, and M Bauduin, "Phenomenology of mutual interference of FMCW and PMCW automotive radars," in *2017 IEEE Radar Conf. (RadarConf)*. IEEE, 2017, pp. 1709–1714.
- [15] Marcus Reiher and Bin Yang, "On the occurrence of ghost targets in linear FMCW radar: A worst case study," in *Proc. IEEE Int. Radar Symp.*, 2008, pp. 1–4.
- [16] Feng Jin and Siyang Cao, "Automotive radar interference mitigation using adaptive noise canceller," *IEEE Trans. Veh. Technol.*, vol. 68, no. 4, pp. 3747–3754, 2019.
- [17] Sharef Neemat, Oleg Krasnov, and Alexander Yarovoy, "An interference mitigation technique for FMCW radar using beat-frequencies interpolation in the STFT domain," *IEEE Trans. Microw. Theory Techn.*, vol. 67, no. 3, pp. 1207–1220, 2019.
- [18] Jianping Wang, Min Ding, and Alexander Yarovoy, "Interference mitigation for FMCW radar with sparse and low-rank Hankel matrix decomposition," *IEEE Trans. Signal Process.*, vol. 70, pp. 822–834, 2022.
- [19] Seongwook Lee, Jung-Yong Lee, and Seong-Cheol Kim, "Mutual interference suppression using wavelet denoising in automotive FMCW radar systems," *IEEE Trans. Intell. Transport. Syst.*, vol. 22, no. 2, pp. 887–897, 2019.
- [20] Arindam Bose, Bo Tang, Mojtaba Soltanalian, and Jian Li, "Mutual interference mitigation for multiple connected automotive radar systems," *IEEE Trans. Veh. Technol.*, vol. 70, no. 10, pp. 11062–11066, 2021.
- [21] Bo Tang, Wenjie Huang, and Jian Li, "Slow-time coding for mutual interference mitigation," in *2018 IEEE Int. Conf. Acoust., Speech Signal Process.* IEEE, 2018, pp. 6508–6512.
- [22] Zhongxiao Jia and GW Stewart, "An analysis of the Rayleigh–Ritz method for approximating eigenspaces," *Mathematics of computation*, vol. 70, no. 234, pp. 637–647, 2001.